Electronic Supplementary Material (ESI) for Physical Chemistry Chemical Physics.

Supporting Information

A Study of Competitive Multiple Hydrogen Bonding Effect and Its Associated Excited-State Proton Transfer Tautomerism

Yi-Ting Chen,[¶,a] Pei-Jhen Wu,[¶,a] Chia-Yu Peng,[¶,b] Jiun-Yi Shen,[a] Cheng-Cheng Tsai,[b] Wei-Ping Hu,[b,*] and Pi-Tai Chou[a,*]

[†]Department of Chemistry and Center for Emerging Material and Advanced Devices, National Taiwan University, Taipei 10617, Taiwan, R.O.C.

[‡]Department of Chemistry and Biochemistry, National Chung Cheng University, Chia-Yi 62102, Taiwan, R.O.C.

Corresponding Author

Email:chop@ntu.edu.tw (P.-T. Chou)
Email: chewph@ccu.edu.tw (W.-P. Hu)

Contents

page

Experimental section

Experimental Section

Synthesis and characterization. All solvents were distilled from appropriate drying agents prior to use. Commercially available reagents were used without further purification unless otherwise stated. All reactions were monitored by TLC. Column chromatography was carried out using silica gel from Merck (230-400 mesh). ^{1}H and ^{13}C NMR spectra were recorded on a Varian Unity 400 spectrometer at 400 MHz and 100 MHz, respectively. Chemical shifts (δ) are recorded in parts per million (ppm) and coupling constants (*J*) are reported in Hertz (Hz). Mass spectra were obtained using a Gas Chromatograph-Mass Spectrometer (Finnigan MAT TSQ-46C GC/MS/MS/ DS).

Synthesis of 1,8-bis(ethoxymethoxy)naphthalene **(2)**. To a solution of naphthalene-1,8-diol (**1**) (1.60 g, 10 mmol, brand: COMBI-BLOCKS) in DMF (12 mL) at 0 °C was added NaH (30 mmol) and stirred for 1 h. A solution of chloromethyl ethyl ether (2.3 mL, 25 mmol) in Et_2O (10 mL) was added to the mixture. After stirring overnight, the reaction mixture was added to water and extracted with Et_2O (20 mL × 3). The organic extracts were combined, dried over anhydrous $MgSO_4$, filtered and concentrated. The residue was purified using column chromatography on silica gel (DCM/hexane) to yield **2** (2.34 g, 85%) as a white solid. ^{1}H NMR (400 MHz, $CDCl_3$): δ 7.47 (d, *J* = 8.4 Hz, 2 H), 7.32 (t, *J* = 7.6 Hz, 2 H), 7.07 (d, *J* = 7.6 Hz, 2 H), 5.32 (s, 4 H), 3.83 (q, 4 H), 1.26 (t, 6 H) ^{13}C NMR (100 MHz, $CDCl_3$): δ 153.7, 137.4, 126.1, 122.5, 112.4, 95.0, 94.4, 64.4, 15.0.ESI-MS: m/z 276 (M^+).

Synthesis of 1,8-bis(ethoxymethoxy)naphthalene-2,7-dicarbaldehyde **(3).** A solution of compound **2** (1.52 g, 5.5 mmol) and Et_2O (10 mL) at 0 °C was added dropwise to a mixture of n-BuLi (2.5 M in hexane, 5.72 mL, 14.2 mmol) and TMEDA (2.12mL, 14.2 mmol) in Et_2O (100 mL) and stirred for 6 h at this temperature. DMF (1.7 mL, 22 mmol) was added to the mixture for stirring overnight (0 °C to r.t.). Water was added to the mixture and the pH7 adjusted using 1.0 N HCl(aq). After extraction with Et_2O, the organic layer was dried over $MgSO_4$, filtered and evaporated. The residue was purified using column chromatography on silica gel (hexane/EA) to yield the **3** (1.11 g, 61%) as an ochre solid. ^{1}H NMR (400 MHz, $CDCl_3$): δ 10.58 (s, 2 H), 7.99 (d, *J* = 8.8 Hz, 2 H), 7.68 (d, *J* = 8.4 Hz, 2 H), 5.27 (s, 4 H), 3.77 (q, 4 H), 1.20 (t, 6H). ^{13}C NMR (100 MHz, $CDCl_3$): δ 190.2, 158.9, 143.5, 128.3, 126.0, 125.7, 121.3, 100.8, 66.7, 15.0. ESI-MS: m/z 332(M^+).

Synthesis of 1,8-dihydroxynaphthalene-2,7-dicarbaldehyde **(DHDA)**. A solution of compound **3** (0.31 g, 1.0 mmol) in CH_2Cl_2 (25 mL) at 0 °C was added dropwise to a mixture of isopropanol (6.4 mL) and HCl (4.8 mL). After stirring for 6 h, the solvent was removed under reduced pressure. The residue was extracted with CH_2Cl_2 and wash with the water, dried over anhydrous $MgSO_4$, filtered and concentrated to yield the DHDA (0.15 g, 69%) as a yellow solid. ^{1}H NMR (400 MHz, $CDCl_3$): δ 12.64 (s, 2 H), 10.15 (s, 2 H), 7.73 (d, J = 8.4 Hz, 2 H), 7.29 (d, J = 8.8 Hz, 2 H).^{13}C NMR (100 MHz, $CDCl_3$) δ 193.3, 164.1, 142.9, 130.3, 119.8, 116.4, 113.8. ESI-MS: m/z 216 $(M+H)^+$.

Spectroscopic Measurements Steady-state absorption spectra were recorded using a Hitachi U-3310 Spectrophotometer, and emission spectra were obtained using an Edinburgh FS920 Fluorimeter. Detailed time-resolved spectroscopic measurements have been reported previously.[52] In brief, nanosecond time-resolved experiments were performed by using an Edinburgh FLS920 time-correlated single photon-counting (TCSPC) system with a pulsed hydrogen-filled lamp as the excitation source. Data were fitted with the sum of exponential functions using a nonlinear least-squares procedure in combination with a convolution method.

Sub-nanosecond to nanosecond time-resolved studies were performed using another TCSPC system (OB-900 L lifetime spectrometer, Edinburgh) with an excitation light source from the second harmonic generation (SHG, 400 nm) of pulse-selected femtosecond laser pulses at 800 nm (Tsunami, Spectra-Physics) and a microchannel plate (MCP) detector. The fluorescence was collected at a right angle with respect to the pump beam path and passed through a polarizer, which was located in front of the detector. The polarization was set at a magic angle (54.7º) with respect to the pump polarization direction to eliminate anisotropy. Similar data analysis and fitting procedures were applied. The temporal resolution, after partial removal of the instrumental time broadening, was ~20 ps.

Ultrafast spectroscopic study of the titled compounds was performed by a femtosecond photoluminescence up-conversion (uPL) system pumped at 400 nm. In this measurement, fluorescence from a rotating sample cell was focused in a BBO crystal and its frequency was summed along with an interrogation gate pulse at a designated delay time with respect to the pump pulse. A half-wave plate was used to set the pump polarization at a magic angle (54.7º) with respect to the gate pulse to prevent the fluorescence anisotropy contributed by solute reorientation. Fluorescence up-conversion data were fitted to the sum of exponential functions convoluted with the instrument response function (IRF). The IRF was determined from the Raman scattering signal and its profile was fitted to a Gaussian function

with a full width at half maximum of ~220 fs.

Computational methodology The structures and energies of the 1,8-dihydroxynaphthalene-2,7-dicarbaldehyde (**DHDA**) molecule and its tautomers in solvents were calculated by the hybrid density functionals B3LYP with the 6-31+G(d,p) basis set for the ground-state (S_0) potential energy surface (PES). Their first excited state structures, energies, vertical $S_0 \rightarrow S_1$ excitation and the $S_1 \rightarrow S_0$ emissions were computed by the time-dependent (TD) approach with the same functional and basis set as in the ground-state calculation. The above B3LYP/6-31+G(d,p) calculation on S_0 were checked by the single-point calculation at MP2/6-31+G(d,p) level on the B3LYP/6-31+G(d,p) geometries and by the full calculation using the M06-2X functional with 6-31+G(d,p) basis set. The solvation effects was considered by using the polarizable continuum model (PCM) in the solvent of cyclohexane. The higher level EOM-CCSD/6-31+G(d,p) calculation was also performed to calculate the relative energies on the S_1 PES using the TD-B3LYP/6-31+G(d,p) geometries. All the calculations were performed using the Gaussian 09 program except that the EOM-CCSD calculation was performed using the MOLPRO program.

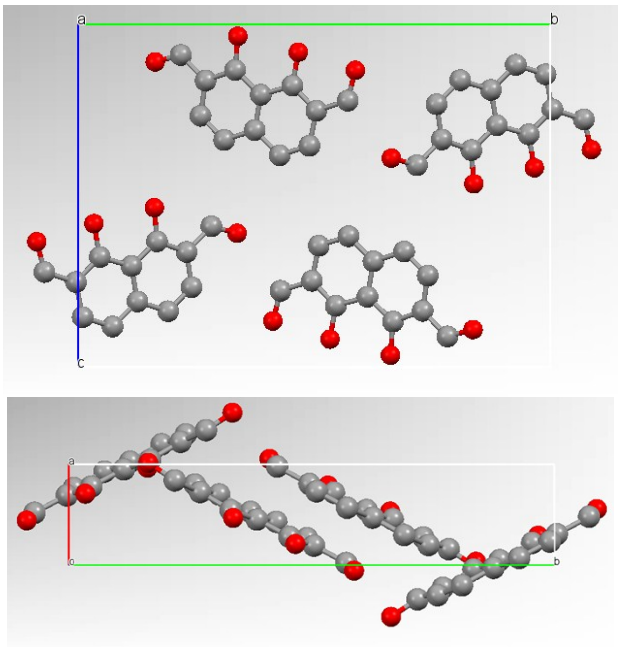

Figure S1. Side views of the packing of **DHDA** in the unit cell.

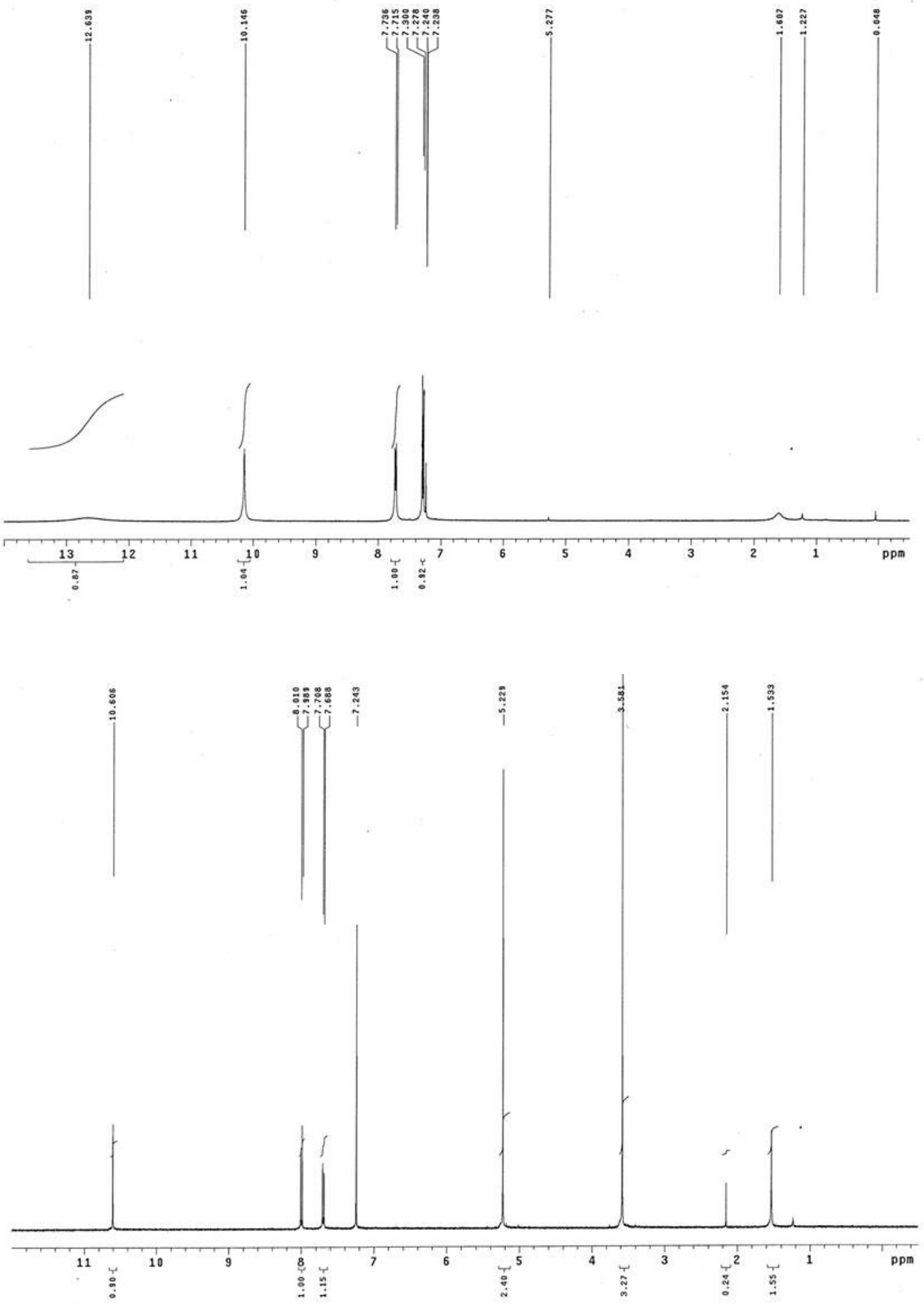

Figure S2. The ^{1}H NMR spectroscopy of **DHDA** (up) and **3**(down) in $CDCl_3$.

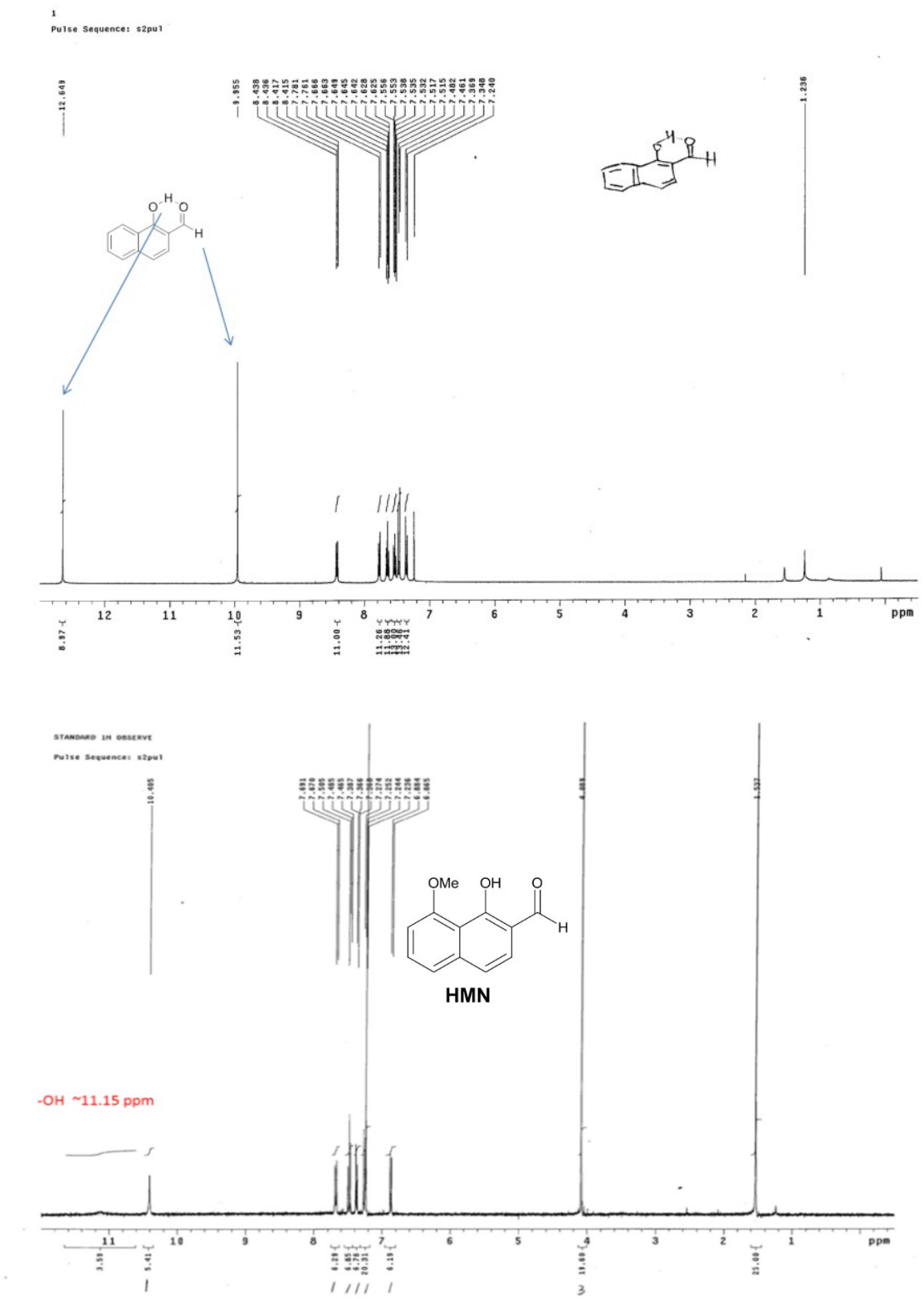

Figure S3. The ^{1}H NMR spectroscopy of **HN** (up) and **HMN** (down) in $CDCl_3$.

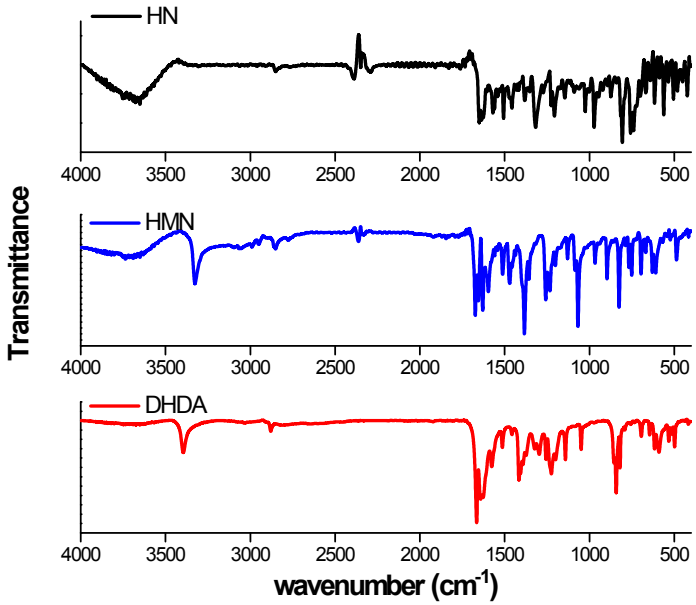

Figure S4. The IR spectra of **HN**, **HMN** and **DHDA** in KBr

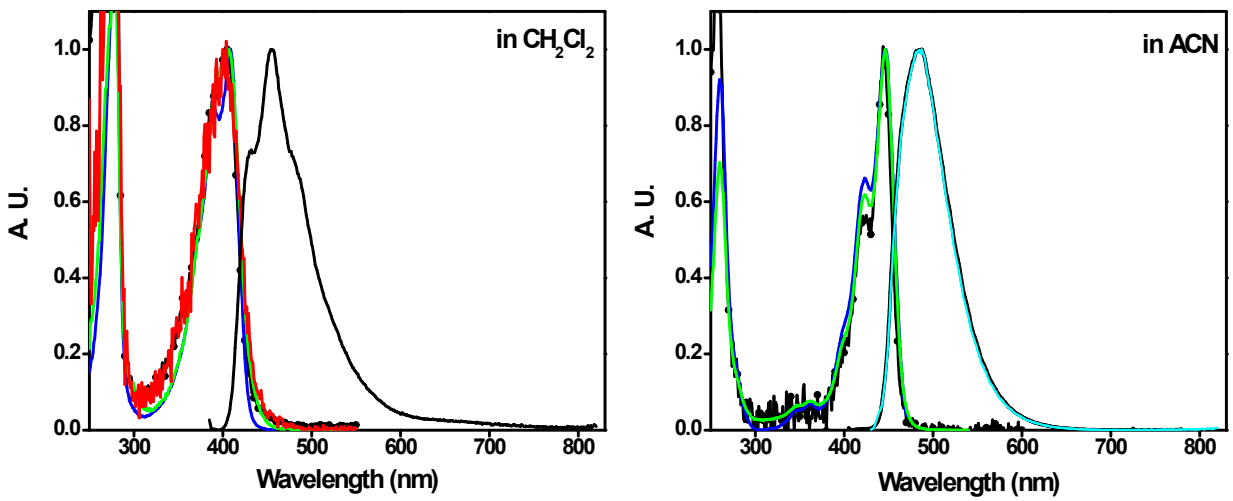

Figure S5. Normalized steady-state absorption (black), excitation spectra (monitor at 470 nm (blue), 550 nm (green) and 700 nm (red in CH_2Cl_2)) and emission spectrum (black, λ_{ex}=380 nm; cyan, λ_{ex}=440) for **DHDA** in the described solvents at room temperature.

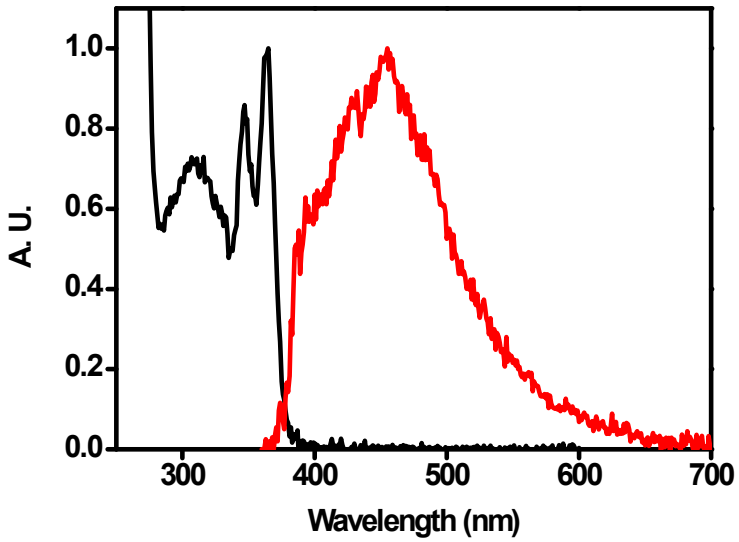

Figure S6. Normalized absorption and emission spectrum for **3** in the cyclohexane.

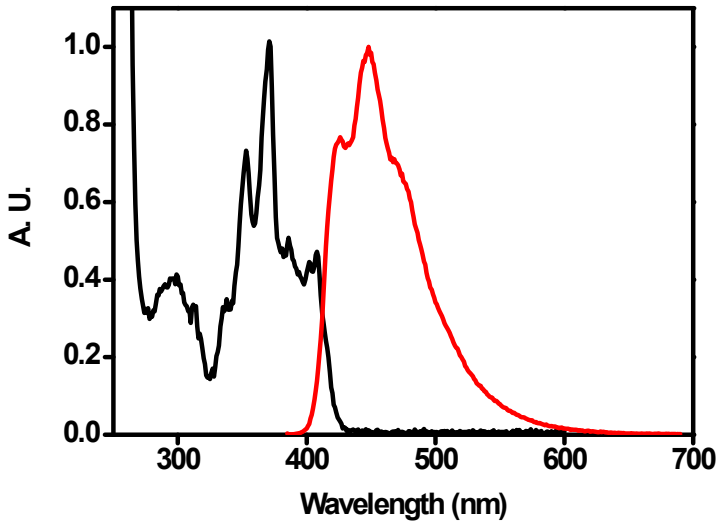

Figure S7. Normalized absorption and emission spectrum for **HMN** in the cyclohexane.

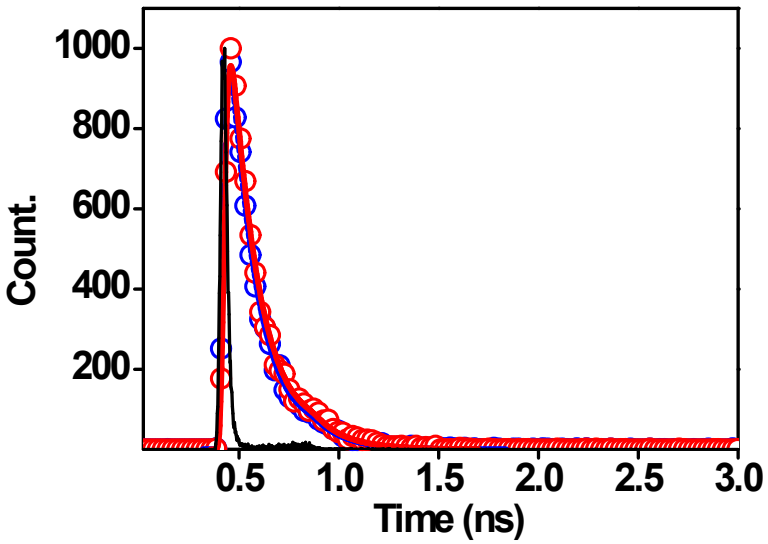

Figure S8. Time-resolved relaxation dynamics of **DHDA** in solid state monitored at 520 nm (blue open circles, ○), and 700 nm, (red open square,□). Solid lines depict the corresponding fitting curves (blue and red) and instrument response function (black).

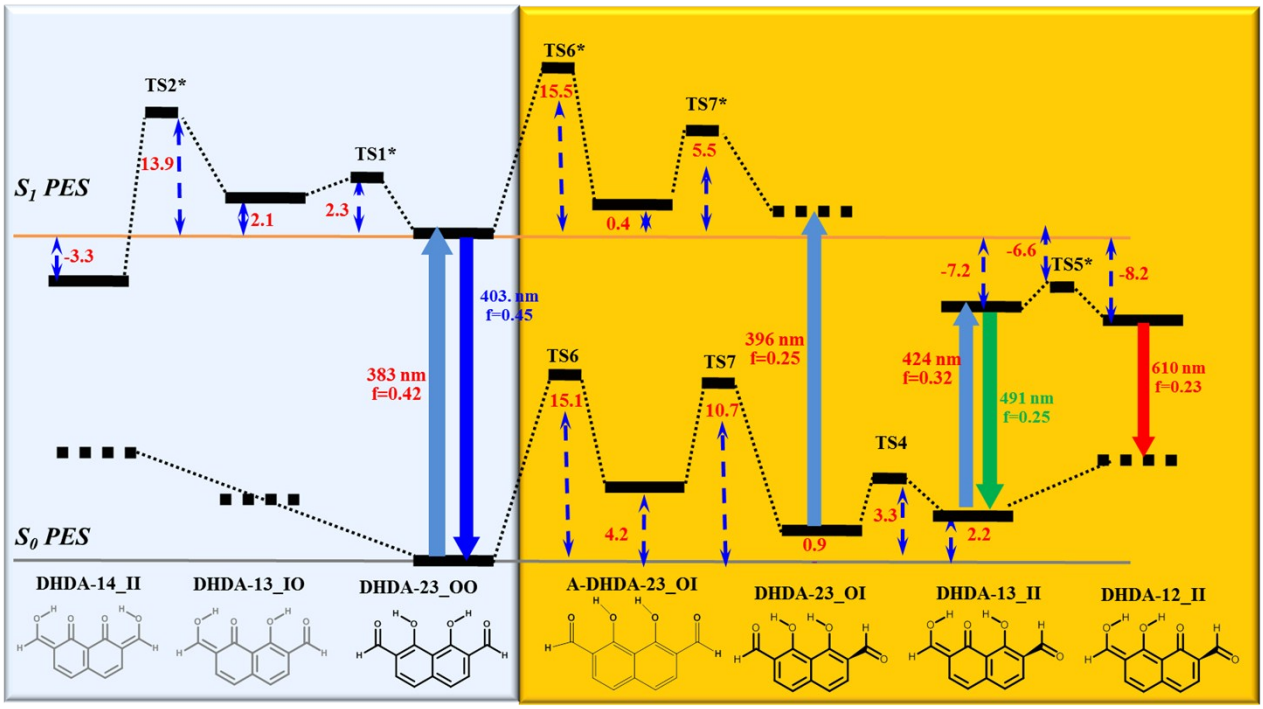

Figure S9. The complete ground (S_0) and the first singlet excited state (S_1) relative energies of **DHDA**.

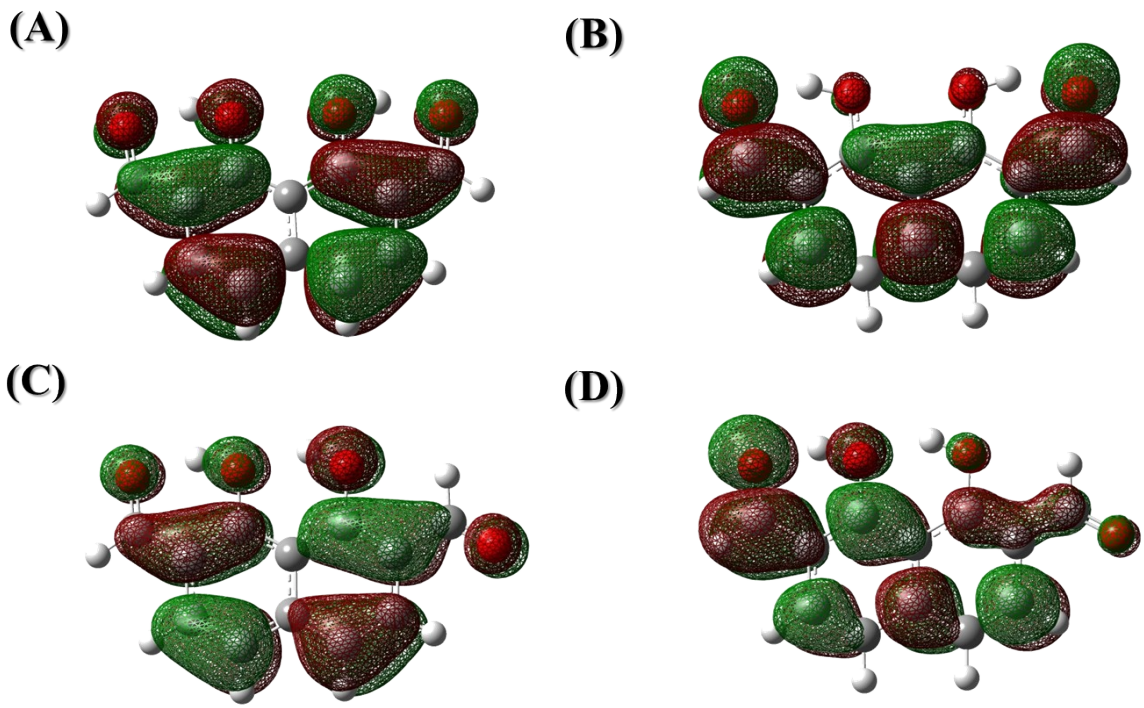

Figure S10. Predicted transition orbitals of DHDA-23_OO and DHDA-23_IO. HOMO (A) and LUMO (B) of DHDA-23_OO; HOMO (C) and LUMO (D) of DHDA-23_OI.

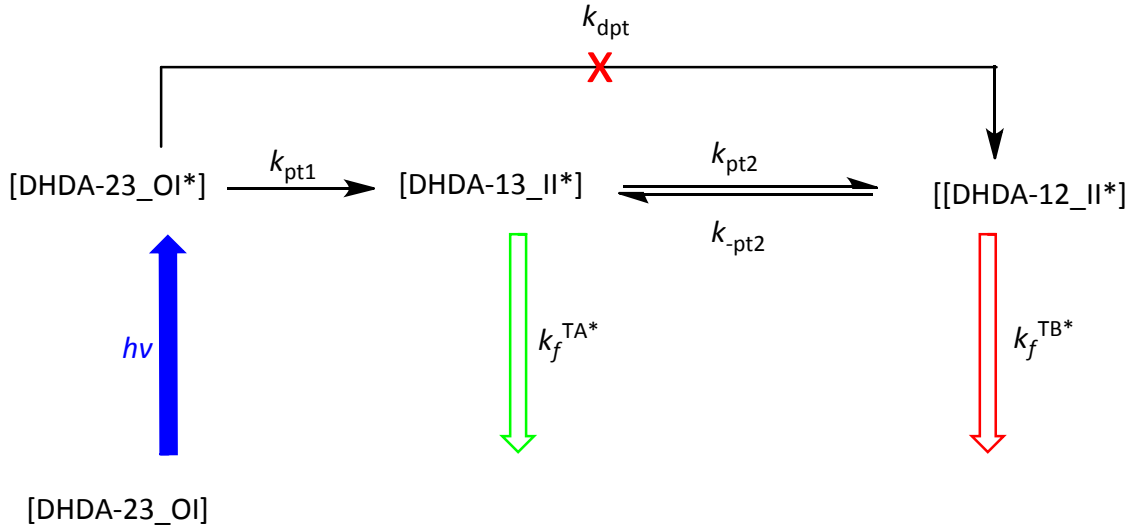

Scheme S1. The proposed mechanism of excited-state double proton transfer for **DHDA-23_OI**. Note that the asterisk * denoted the electronically excited state.

In **Scheme S1** we also draw a concerted PT pathway (k_{dpt}) but specify that this process is unlikely to take place according to the kinetic data. This viewpoint is also supported by theoretical arguments based on the PES landscape, concluding that the concerted PT pathway is thermally unfavorable.

Based on the experimental data we conclude the rate of first proton transfer k_{pt1} (**DHDA-23_OI*** →**DHDA-13_II***) to be faster than the system response of (150 fs)$^{-1}$. Therefore, in a time frame of several ps of interest, it can be assumed that at t ~ 0 (< few hundred fs in reality) N* has been depopulated to ~zero and **DHDA-13_II*** is instantaneously populated (**DHDA-13_II*** = **[DHDA-13_II*]$_0$** at t = 0). Therefore, the time-dependent **DHDA-13_II*** and **DHDA-12_II***, specified as [DHDA-13_II*] and [DHDA-12_II*], respectively, can be expressed as

$$\frac{d[\text{DHDA-13\_II*}]}{dt} = -(k_f^{TA*} + k_{pt2}) \cdot [\text{DHDA-13\_II*}] + k_{-pt2}[\text{DHDA-12\_II*}] \quad \text{.....(1)}$$

$$\frac{d[\text{DHDA-12\_II*}]}{dt} = -(k_f^{TB*} + k_{-pt2}) \cdot [\text{DHDA-12\_II*}] + k_{pt2}[\text{DHDA-13\_II*}] \quad \text{.....(2)}$$

where k_f^{TA*} and k_f^{TB*} are the sum of non-ESIPT decay rate for TA* and TB*, respectively. The differential Eqs. (1) and (2) can be solved by Laplace transformation to obtain Eqs. (3) and (4)

$$[\text{DHDA-13\_II*}] = \frac{[\text{DHDA-13\_II*}]_0}{\lambda_2 - \lambda_1} \cdot [(\lambda_2 - X) \cdot e^{-\lambda_1 t} + (X - \lambda_1) \cdot e^{-\lambda_2 t}] \quad \text{.....(3)}$$

$$[\text{DHDA-12\_II*}] = \frac{k_{\text{pt2}} \cdot [\text{DHDA-13\_II*}]_0}{\lambda_2 - \lambda_1} \cdot [e^{-\lambda_1 t} - e^{-\lambda_2 t}] \quad \text{.....(4)}$$

Where $\lambda_{1,2} = \frac{1}{2}[(X+Y) \mp \sqrt{(X-Y)^2 + 4 \cdot k_{\text{pt2}} \cdot k_{-\text{pt2}}}]$ .....(5)

$X = k_{\text{pt2}} + k_f^{\text{TA*}}, Y = k_{-\text{pt2}} + k_f^{TB*}$ .....(6)

The experimental results also draw the conclusion that the rate of forward DHDA-13_II* $\rightarrow$ DHDA-12_II* (k_{pt2}) and reverse DHDA-12_II* $\rightarrow$ DHDA-13_II* ($k_{\text{-pt2}}$) proton transfer is much larger than k_f^{TA*} and $k_f^{\text{TB*}}$. Under the condition of $k_{\text{pt2}}, k_{\text{-pt2}} >> k_f^{\text{TA*}}, k_f^{\text{TB*}}$, it is thus reasonable for us to claim the pseudo equilibrium between DHDA-13_II* and DHDA-12_II* prior to their corresponding emission. As a result, $X \approx k_{\text{pt2}}$ and $Y \approx k_{-\text{pt2}}$ and Eqs. (5) can be written as follows.

$$\lambda_1 = \frac{1}{\tau_1} = \frac{k_f^{\text{TA*}} \cdot k_{-pt2} + k_f^{\text{TB*}} \cdot k_{pt2}}{k_{-pt2} + k_{pt2}} = \frac{k_f^{\text{TA*}} + k_f^{\text{TB*}} \text{K}_{\text{eq}}}{1 + \text{K}_{\text{eq}}}, \lambda_2 = \frac{1}{\tau_2} = k_{\text{pt2}} + k_{-\text{pt2}} \quad \text{.....(7)}$$

The pre-exponential factors in Eqs 3 for the [DHDA-13_II*] can be derived further as

$$\text{A}_1 \approx \frac{[\text{DHDA-13\_II*}]_0 \cdot (X - \lambda_1)}{\lambda_2 - \lambda_1} \approx \frac{k_{\text{pt2}}}{k_{\text{pt2}} + k_{-\text{pt2}}} \quad \text{.....(8)}$$

$$\text{A}_2 \approx \frac{[\text{DHDA-13\_II*}]_0 \cdot (\lambda_2 - X)}{\lambda_2 - \lambda_1} \approx \frac{k_{-\text{pt2}}}{k_{\text{pt2}} + k_{-\text{pt2}}} \quad \text{.....(9)}$$

The ratio between A_1 and A_2, i.e. A_1/A_2 is thus derived to be $k_{\text{pt2}}/k_{\text{-pt2}}$, which is equivalent to the equilibrium constant K_{eq} ($=k_{\text{pt2}}/k_{\text{-pt2}}$) between DHDA-13_II* and DHDA-12_II* species. We then further convert the time-resolved concentration expression (Eqs 3, 4) to the time-resolved fluorescence intensity of DHDA-13_II* and DHDA-12_II*, denoted as $[\text{DHDA-13\_II*}]_{\text{f}}$ and $[\text{DHDA-12\_II**}]_{\text{f}}$. This is done by multiplying the instrument factor (I_0) and the fluorescence radiative decay rate constant $k_r^{\text{TA*}}$ and $k_r^{\text{TB*}}$ for DHDA-13_II* and DHDA-12_II**, respectively, giving Eqs. (10) and (11), which is essentially identical with equation (I) in the text.

$$[\text{DHDA-13\_II*}]_{\text{f}} = \frac{I_0 \cdot k_r^{\text{TA*}} \cdot [\text{DHDA-13\_II*}]_0}{\lambda_2 - \lambda_1} \cdot [(\lambda_2 - X) \cdot e^{-\lambda_1 t} + (X - \lambda_1) \cdot e^{-\lambda_2 t}] \quad \text{.....(10)}$$

$$[\text{DHDA-12\_II*}]_{\text{f}} = \frac{I_0 \cdot k_r^{\text{TB*}} \cdot k_{\text{pt2}} \cdot [\text{DHDA-13\_II*}]_0}{\lambda_2 - \lambda_1} \cdot [e^{-\lambda_1 t} - e^{-\lambda_2 t}] \quad \text{.....(11)}$$

Table S1. Crystal data and structure refinement for **DHDA**

CCDC no.	1563984	
Empirical formula	$C_{12}H_8O_4$	
Formula weight	216.18	
Temperature	200(2) K	
Wavelength	0.71073 Å	
Crystal system	Monoclinic	
Space group	$P2_1/n$	
Unit cell dimensions	a = 3.7960(3) Å	α= 90°.
	b = 18.3816(13) Å	β= 90.367(5)°.
	c = 13.3342(10) Å	γ = 90°.
Volume	930.40(12) $Å^3$	
Z	4	
Density (calculated)	1.543 Mg/m^3	
Absorption coefficient	0.117 mm^{-1}	
F(000)	448	
Crystal size	0.400 x 0.100 x 0.100 mm^3	
Theta range for data collection	1.527 to 27.488°.	
Index ranges	-4<=h<=4, -23<=k<=23, -17<=l<=17	
Reflections collected	5536	
Independent reflections	2091 [R(int) = 0.0408]	
Completeness to theta = 25.242°	99.9 %	
Absorption correction	Semi-empirical from equivalents	
Max. and min. transmission	0.988 and 0.945	
Refinement method	Full-matrix least-squares on F^2	
Data / restraints / parameters	2091 / 0 / 148	
Goodness-of-fit on F^2	1.020	
Final R indices [I>2sigma(I)]	R1 = 0.0543, wR2 = 0.1389	
R indices (all data)	R1 = 0.0922, wR2 = 0.1608	
Extinction coefficient	n/a	
Largest diff. peak and hole	0.231 and -0.214 $e.Å^{-3}$	

Table S2. Bond lengths for the **DHDA** crystal structure

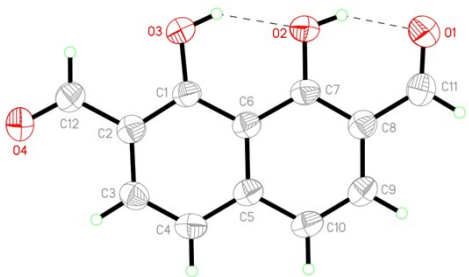

Bond Lengths (Å)			
O(1)-C(11)	1.232(3)	C(4)-C(5)	1.411(3)
O(2)-C(7)	1.344(2)	C(5)-C(10)	1.425(3)
O(3)-C(1)	1.352(2)	C(5)-C(6)	1.427(3)
O(4)-C(12)	1.221(3)	C(6)-C(7)	1.427(3)
C(1)-C(2)	1.397(3)	C(7)-C(8)	1.394(3)
C(1)-C(6)	1.431(3)	C(8)-C(9)	1.413(3)
C(2)-C(3)	1.412(3)	C(8)-C(11)	1.450(3)
C(2)-C(12)	1.462(3)	C(9)-C(10)	1.365(3)
C(3)-C(4)	1.364(3)		

Table S3. Hydrogen bond distances and angles for **DHDA** crystal structure

D-H···A	d(D-H)/Å	d(H···A)/Å	d(D···A)/ Å	<(DHA)/ °
O(2)-H(2)...O(1)	0.84	1.78	2.532(2)	148.5
O(3)-H(3)...O(2)	0.84	1.90	2.629(2)	145.0

Table S4. Calculated ground-state (S_0) energetics in kcal/mol of **DHDA** system in cyclohexane solvent. The listed relative energies correspond to those in Figures 5 and S8, and the zero of energy is DHDA-23_OO.

	B3LYP/6-31+G(d,p)	MP2/6-31+G(d,p)// B3LYP/6-31+G(d,p)	M06-2X/6-31+G(d,p)
DHDA-23_OO	0.0	0.0	0.0
DHDA-23_OI	0.9	-0.9	-0.01
DHDA-13_II	2.2	3.6	2.6
A-DHDA-23_OI	4.2	2.6	3.5
TS4	3.3	4.1	3.1
TS6	15.1	11.7	13.2
TS7	10.7	6.0	9.3

Table S5. Calculated first excited state (S_1) energetics in kcal/mol of **DHDA** system in cyclohexane solvent. The listed relative energies correspond to those in Figures 5 and S8, and the zero of energy is DHDA-23_OO*.

	TD-B3LYP/6-31+G(d,p)	EOM-CCSD/6-31+G(d,p) // TD-B3LYP/6-31+G(d,p)
DHDA-14_II*	-3.3	4.3
DHDA-13_IO*	2.1	3.1
DHDA-23_OO*	0.0	0.0
DHDA-13_II*	-7.2	-4.9
DHDA-12_II*	-8.2	-8.0
A-DHDA-23_OI*	0.4	-
TS1*	2.3	3.3
TS2*	13.9	15.2
TS5*	-6.6	-3.5
TS6*	15.5	-
TS7*	5.5	-